Role of non-magnetic spacers in the magnetic interactions of antiferromagnetic topological insulators MnBi₄Te₇ and MnBi₂Te₄

Bing Li,^{1,2,*} D. M. Pajerowski,³ J.-Q. Yan,³ and R. J. McQueeney^{1,2}

¹ Ames National Laboratory, Ames, IA, 50011, USA

² Department of Physics and Astronomy, Iowa State University, Ames, IA, 50011, USA

³ Oak Ridge National Laboratory, Oak Ridge, TN, 37831, USA

(Dated: October 29, 2024)

MnBi₄Te₇ belongs to a family of antiferromagnetic topological insulators. It forms a natural heterostructure of magnetic (septuple) and non-magnetic (quintuple) topological blocks. Here, we explore the magnetism and magnetic interactions in this compound using inelastic neutron scattering. We find that the interlayer magnetic coupling is much weaker in MnBi₄Te₇ as compared to MnBi₂Te₄ due to the insertion of non-magnetic quintuple layers in the former. However, other key magnetic energy scales residing within a single septuple block, the single-ion anisotropy and long-range intralayer exchanges, are essentially the same. This identifies a transferable set of magnetic interactions applicable to the extended family of magnetic topological insulators based on MnBi₂Te₄-Bi₂Te₃ heterostructures.

I. INTRODUCTION

The MnBi₂Te₄ (MBT) is the first known antiferromagnetic topological insulator [1–3] and has been utilized as a platform to interrogate the novel phenomena in topological phases such as axion and Chern insulators [4–8]. The key to accessing these topological properties is the van der Waals coupling between structural blocks, resulting in weak interlayer antiferromagnetic coupling. Combined with an uniaxial magnetic anisotropy of the Mn sublattice, MBT provides easily accessible metamagnetic spinflop and forced ferromagnetic phases that host unique topological phenomena [9].

Much less explored are the extended family of $MnBi_{2+2n}Te_{4+3n}$ compounds where MBT septuple blocks are separated by n non-magnetic Bi_2Te_3 quintuple topological insulator (TI) blocks [10–15]. A single septuple block is ferromagnetic (FM), while the interlayer magnetic coupling is antiferromagnetic (AF), at least for n = 0, 1, and 2. The insertion of non-magnetic spacer blocks increases the Mn sublattice interlayer distance and, therefore, is expected to reduce the interlayer magnetic coupling, affecting the landscape of magnetic phases and magnetization dynamics [9, 14, 16–19, 21]. The MBT family provides a means for controlled studies of the magnetization dynamics where interlayer couplings can be tuned from weak (for MnBi₂Te₄) to essentially zero (for $MnBi_8Te_{13}$) [16]. In the latter n=3 system, long-range dipolar interactions dominate the interlayer coupling, resulting in fragile ferromagnetism [20].

It has been suggested large n MBT compounds form a new class of magnets, called single-layer magnets [16], which consist of a periodic array of magnetic layers with vanishing interlayer coupling. Thus, in addition to the interesting topological properties, the MBT family also allows for the exploration of the interplay between dimensionality and magnetism in these unique van der Waals bonded natural heterostructures.

In the quest to understand the evolution towards single-layer magnets, here we describe inelastic neutron scattering (INS) measurements on the n=1 compound MnBi₄Te₇. Comparison of these results to similar measurements on the n=0 compound MnBi₂Te₄ [22] reveals several trends in the magnetic energy scales of these compounds. We find that MnBi₄Te₇ has a strongly suppressed interlayer spin wave bandwidth and a reduction in the spin gap compared to MnBi₂Te₄. Both observations are consistent with vanishing interlayer exchange coupling and a transferable single-ion anisotropy. Without the influence of the interlayer couplings, the interactions within a single septuple block could be more reliably determined using the linear spin wave theory (LSWT) analysis based on the Heisenberg model. This analysis confirms that long-range and competing intralayer interactions found in MnBi₂Te₄ are intrinsic to the septuple blocks in all MBT family members [22, 23].

Overall, this suggests that $MnBi_4Te_7$ and successive n > 1 MBT family members are quite close to the 2D limit. Considering that INS is a bulk measurement, we propose that $MnBi_4Te_7$ serves as a suitable system to probe 2D magnetism, which is not only interesting theoretically but also relevant for the development of few-layer magnetic TI devices [19, 24–26].

II. EXPERIMENTAL DETAILS

Single-crystal samples of MnBi₄Te₇ and MnBi₂Te₄ were grown out of a Bi-Te flux [12]. The elemental analysis and X-ray and neutron diffraction results reveal that the Mn site hosts extra Bi and Mn vacancies, giving a chemical formula of Mn_{0.8}Bi_{4.2}Te₇. MnBi₂Te₄ crystallizes in space group $R\bar{3}m$ (#166), with lattice parameters a=b=4.33 Å, c=40.91 Å whereas MnBi₄Te₇

^{*} Current address: Oak Ridge National Laboratory, Oak Ridge, TN, 37831, USA

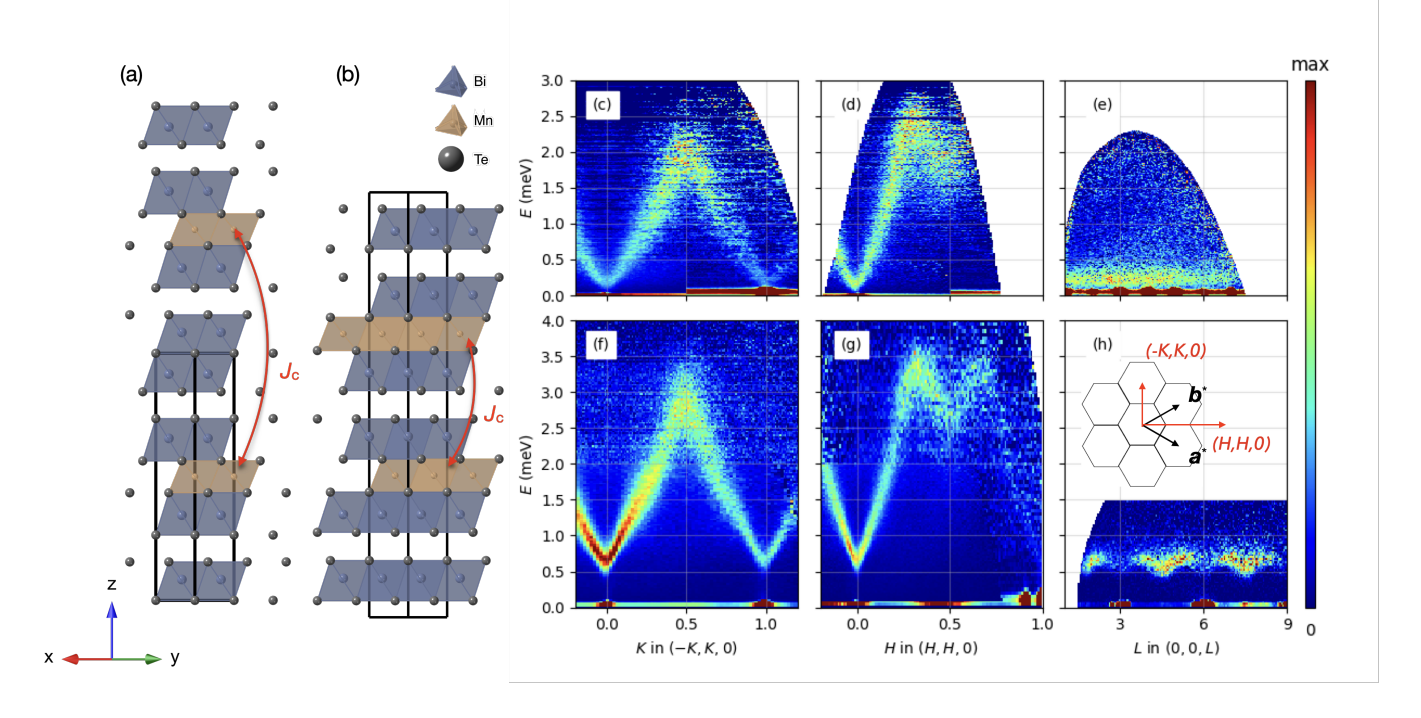


FIG. 1. Crystal structure of (a) MnBi₄Te₇ and (b) MnBi₂Te₄ with J_c indicating the distance of the nearest interlayer neighbor. (c-e) Spin waves in MnBi₄Te₇ measured at T=2 K with $E_{\rm i}=3.32$ meV. Measurement with $E_{\rm i}=1.55$ meV is overlaid on top in (c) and (d) for better visualization of the spin gap at low E. (f-h) Spin waves in MnBi₂Te₄ measured at T=2 K with $E_{\rm i}=6.6$ meV, with $E_{\rm i}=3.3$ meV measurement overlaid on top in (f) and (g). The intensity in (c-h) is multiplied by energy transfer E to enhance the contrast at higher E. Inset of (h) shows the 2D projection of the Brillouin zone and the high-symmetry directions.

crystallizes in space group $P\bar{3}m1$ (#164), with lattice parameters a=b=4.366 Å, c=23.80 Å. The essential difference between the two chemical structures is the close-packed stacking of magnetic Mn sublattice in the former and the simple hexagonal stacking in the latter. A comparison of the two crystal structures is shown in Fig. 1(a) and (b).

For both compounds, the 2D projection of the Brillouin zone is hexagonal and we define reciprocal space vectors $\mathbf{q} = \frac{4\pi}{\sqrt{3}a}(H\hat{\mathbf{a}}^* + K\hat{\mathbf{b}}^*) + \frac{2\pi}{c}L\hat{\mathbf{c}}^*$ and special points $\Gamma = (0,0,0), M = (1/2,0,0), K = (1/3,1/3,0)$. SQUID measurements for MnBi₄Te₇ confirm that AFM ordering occurs at $T_{\rm N} = 13.7$ K and neutron diffraction finds a magnetic propagation vector of $\boldsymbol{\tau} = (0,0,\frac{1}{2})$, consistent with the A-type AFM order [12]. Previous reports of MnBi₂Te₄ find $T_{\rm N} = 24.7$ K and $\boldsymbol{\tau} = (0,0,\frac{3}{2})$ for the A-type order of Mn layers with rhombohedral stacking [3].

Similar to MnBi₂Te₄, the INS measurements on MnBi₄Te₇ were performed using the Cold Neutron Chopper Spectrometer (CNCS) at the Spallation Neutron Source in Oak Ridge National Laboratory. Co-aligned single-crystal samples with a total mass of 503.7 mg [27] were mounted to a top-loading orange cryostat. Measurements were performed using the incident energies $E_{\rm i}=3.32$ and 1.55 meV at base temperatures T=2 K. Measurements at higher temperatures were also taken for the estimation of background signals.

III. RESULTS

Spin waves along high-symmetry directions in $\mathrm{MnBi_4Te_7}$ are shown in Fig. 1(c-e), compared to spin waves in $\mathrm{MnBi_2Te_4}$ shown in Fig. 1(f-h) which are originally reported in Ref. [22]. The intensity is multiplied by energy transfer E to enhance the contrast at higher E. Square brackets are used to denote the range of summation in \mathbf{Q} in reciprocal lattice units. Three orthogonal axes used to denote \mathbf{q} are (H,H,0), (-K,K,0), and (0,0,L). For $\mathrm{MnBi_4Te_7}$ in Fig. 1(c) and (d), L=[2,6]. H=[-0.05,0.05] in (c), and K=[-0.05,0.05] in (d). In (e), H=K=[-0.04,0.04]. For $\mathrm{MnBi_2Te_4}$ in Fig. 1(f) and (g), L=[0,20] for $E_{\rm i}=6.6$ meV data and L=[3,12] for $E_{\rm i}=3.3$ meV data. H=[-0.05,0.05] in (f), and K=[-0.05,0.05] in (g). In (h), H=K=[-0.02,0.02].

Comparison of Figs. 1(c) with 1(f) and Figs. 1(d) with 1(g) indicate that the in-plane dispersions of $\mathrm{MnBi_4Te_7}$ and $\mathrm{MnBi_2Te_4}$ are quite similar. One obvious difference is the slightly lowered spin wave energy maximum (from 3.3 meV to 2.3 meV), and concomitantly the smaller spin gap in $\mathrm{MnBi_4Te_7}$. A comparison of the interlayer dispersions along L in Figs. 1(e) with 1(h) highlights that the interlayer coupling is strongly reduced in $\mathrm{MnBi_4Te_7}$.

We discuss these features of the spin wave spectrum

using LSWT based on the following Heisenberg model,

$$\mathcal{H} = \sum_{\langle ij\rangle,\parallel} J_{ij} \mathbf{S}_i \cdot \mathbf{S}_j - D \sum_i (S_i^z)^2.$$
 (1)

This model is similar to that used in the analysis of MnBi_2Te_4 [22]. The difference is that we use a 2D model for MnBi_4Te_7 where the interlayer coupling terms $J_c \sum_{\langle ij \rangle, \perp} \mathbf{S}_i \cdot \mathbf{S}_j$ are not included. In the next section, we justify this choice by showing that the reduced dispersion along L is too small to resolve J_c with our current data.

A. Interlayer couplings

In Fig. 2, the experimental data of the interlayer dispersion is compared to simulations of the data from linear spin wave theory. For MnBi₂Te₄, one finds that the AFM interlayer coupling has two effects. It creates an oscillatory dispersion along (0,0,L) [Fig. 2(c)] as well as a variation of scattering intensities [Fig. 2(d)]. In the latter case, the intensities having maxima at $L = 3n \pm \frac{3}{2}$ and minima at L = 3n which result from the AFM propagation vector of $\boldsymbol{\tau} = (0,0,3/2)$, corresponding to staggered magnetization of hexagonal close-packed magnetic layers.

In MnBi₄Te₇, however, neither of the two effects are clearly observed. Analysis on the spin wave dispersion along (0,0,L) gives a single-ion anisotropy $SD_z =$ 0.077(1) meV, similar to the value $SD_z = 0.0814$ meV in MnBi₂Te₄ reported in Ref. [22], and an unstable interlayer interaction $SJ_c = 0.001(1)$ meV [27]. Integrated intensities at low E = [0.15, 0.35] meV are plotted in Fig. 2(b) for $MnBi_4Te_7$ along (0,0,L) together with the simulated intensities with $SJ_c = 0$ and $SJ_c = 0.02$ meV. Due to the simple stacking of hexagonal magnetic layers in MnBi₄Te₇, the intensity maxima are expected at $L=n\pm\frac{1}{2}$. However, no distinctive intensity variations are observed with the current counting statistics. For example, with $SJ_c \geq 0.02$ meV, Fig 2(b) shows that the variation of intensities should be significant enough to be observed. Therefore we estimate an upper limit of $SJ_{c} = 0.02 \text{ meV}$ for the interlayer coupling in MnBi₄Te₇.

It is worth mentioning that the difference in magnetic layer stacking results in each Mn ion in MnBi₄Te₇ having only two interlayer nearest-neighbors, whereas in MnBi₂Te₄ each Mn has six. Thus, the upper limit of the energy scale of the total interlayer coupling in MnBi₄Te₇ is at least an order of magnitude smaller than MnBi₂Te₄.

$$\frac{2J_c^{147}}{6J_c^{124}} = \frac{2 \times 0.02}{6 \times 0.065} \lesssim 0.10. \tag{2}$$

B. Spin gap

To investigate the single-ion anisotropy D in MnBi₄Te₇, cuts were made as functions of energy trans-

fer E for data sets with different incident neutron energies. Figs. 3(a) and (b) show INS intensities at the bottom of the magnon band (magnetic Γ point) $\mathbf{q}=(0,0,2.5)$ (r.l.u.), with the summation range H=[-0.04,0.04],~K=[-0.03,0.03] and L=[2.3,2.7]. The peak at $\Delta\approx0.2$ meV corresponds to the spin gap. Intensities at $\mathbf{q}=(0.3,0,2.5)$ with the summation range of H offset to [0.26,0.34] are used to estimate background signals from incoherent scattering. Whereas the data with $E_{\rm i}=3.32$ meV has a coarser resolution than data with $E_{\rm i}=1.55$ meV (orange and red), both data sets give a consistent estimate for the spin gap energy. This can be compared to the $\Delta\approx0.53$ meV for MnBi₂Te₄ as shown in Fig. 3(b) (brown).

However, in contrast to MnBi₂Te₄, there is no clean gap in MnBi₄Te₇ where magnetic scattering intensities are completely absent. The finite spectral weight that is observed down to $E\approx 0$ is not only a consequence of the instrumental resolution, considering that the resolution linewidth at E=0 is about 0.04 meV when $E_{\rm i}=1.55$ meV. Rather, the broadening is caused by the intrinsic damping of the magnons that can be closely approximated as critically damped harmonic oscillators, using the spectral function,

$$F(E) \propto \frac{E \cdot \Gamma}{(E^2 - E_0^2)^2 + (E \cdot \Gamma)^2},\tag{3}$$

where the damping factor Γ satisfies $E_0^2 \geq \Gamma^2/4$. An accurate estimation of the spin gap and the single-ion anisotropy require 2D fitting of the INS spectra with energy-resolution and q-binning effects taken into consideration as performed in section III C.

C. Intralayer couplings

Given the two-dimensional nature of the spin excitations in MnBi₄Te₇ with $J_c \approx 0$, we determine the intralayer magnetic couplings and single-ion anisotropy by using the reduced χ^2 analysis to compare the experimental and simulated spin wave intensities along (-K, K, 0) and (H, H, 0). Starting with Eqn. (1), the analytical expression for spin wave dispersion is given by

$$\begin{split} E(\boldsymbol{q}) &= \sqrt{A(\boldsymbol{q})^2 - B(\boldsymbol{q})^2}, \\ A(\boldsymbol{q}) &= S\left(J(\boldsymbol{q}) + \frac{1}{2}J(\boldsymbol{q} + \boldsymbol{\tau}) + \frac{1}{2}J(\boldsymbol{q} - \boldsymbol{\tau}) - 2J(\boldsymbol{\tau})\right) + 2SD, \\ B(\boldsymbol{q}) &= S\left(J(\boldsymbol{q}) - \frac{1}{2}J(\boldsymbol{q} + \boldsymbol{\tau}) - \frac{1}{2}J(\boldsymbol{q} - \boldsymbol{\tau})\right). \end{split}$$

$$\tag{4}$$

Here $J(\mathbf{q}) = \sum_{j} J_{0j} e^{i\mathbf{q}\cdot\mathbf{R}_{j}}$ is the Fourier transformation of all neighboring magnetic interactions J_{ij} for a given atom at site i, and $\boldsymbol{\tau} = (0,0,\frac{1}{2})$ is the magnetic propagation vector.

The spin wave intensity I(q, E) is proportional to the sum of the transverse components of the dynamic spin-

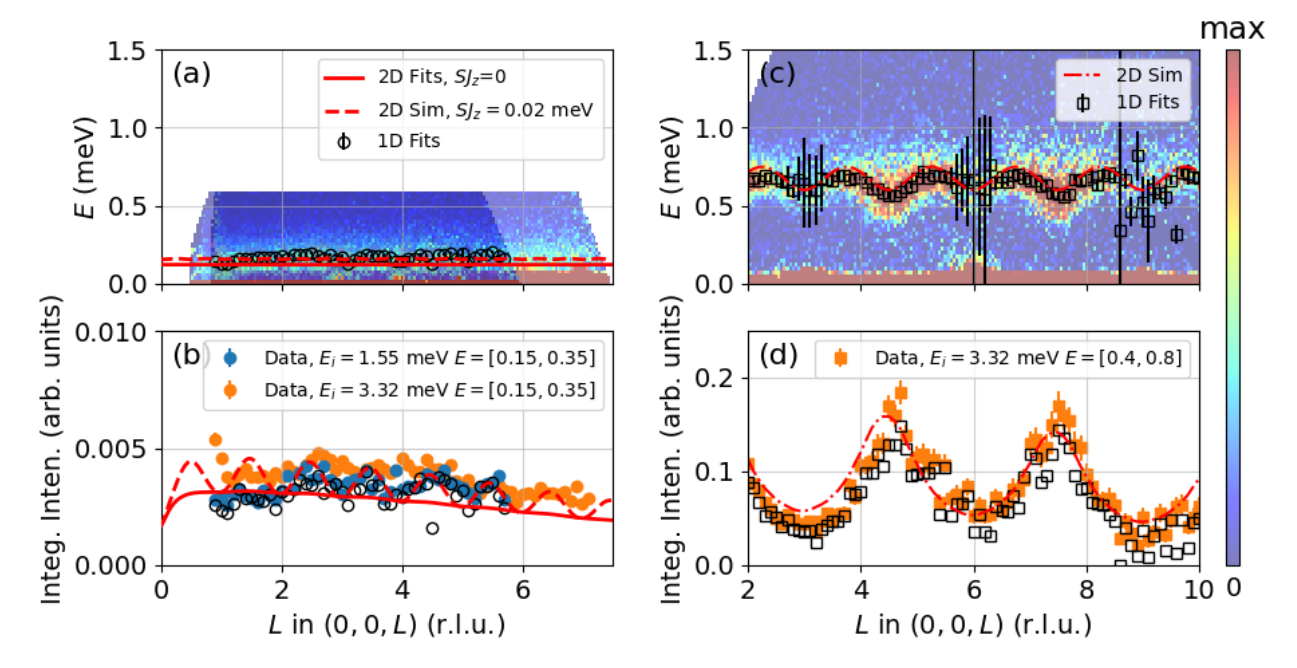


FIG. 2. Integrated INS intensities and spin wave dispersion along (0,0,L) direction for MnBi₄Te₇ (a) and MnBi₂Te₄ (c), similarly to data plotted in Fig. 1(e) and (f). Data with $E_i = 1.55$ meV are overplotted on data with $E_i = 3.32$ meV in (a). (b) and (d) show intensity variation when summed over the energy range E = [0.15, 0.35] meV and E = [0.4, 0.8] meV for MnBi₄Te₇ and MnBi₂Te₄, respectively. Black open symbols with error bars are peak centers in (a) and (c), and integrated intensity in (b) and (d), obtained from fitting individual constant-Q line cuts. (circles for MnBi₄Te₇ and squares for MnBi₂Te₄.) The large error bars in (c) result from the vanishing intensities when approaching E = 3n. Red curves show the simulated dispersion and intensity variation from fitting to the 2D slice of data. Notice that 1D and 2D fitting give consistent results in MnBi₂Te₄. Therefore, the intensity variation is used for an estimation of the upper limit of the interlayer interaction E = 3n shown in (b).

spin correlation function $S^{xx}(q, E)$ and $S^{yy}(q, E)$, where

$$S^{xx}(\boldsymbol{q}, E) = S^{yy}(\boldsymbol{q}, E)$$

$$= S \frac{A(\boldsymbol{q}) - B(\boldsymbol{q})}{E(\boldsymbol{q})} \delta(E - E(\boldsymbol{q})) (1 - e^{-\frac{E}{k_{\mathrm{B}}T}})^{-1}, \quad (5)$$

and the INS spin wave intensity I(q, E) is,

$$I(q, E) = S|f(q)|^{2} \frac{A(q) - B(q)}{E(q)} (1 + \hat{q}_{z}^{2})$$

$$\frac{E \cdot \Gamma}{(E^{2} - E_{0}^{2})^{2} + (E \cdot \Gamma)^{2}} (1 - e^{-\frac{E}{k_{B}T}})^{-1}. \quad (6)$$

 $f(\boldsymbol{q})$ is the magnetic form factor of Mn²⁺ ion, \hat{q}_z is the z component of the unit vector in \boldsymbol{q} direction and $(1-e^{-\frac{E}{k_{\rm B}T}})^{-1}$ is the Bose thermal factor. The δ -function in Eqn. (5) is replaced by the spectral function in Eqn. (3).

One of technical challenges for INS experiment on MnBi₄Te₇ is that, since Bi and Te atoms are both heavy, the atomic percentage of Mn is much lower compared to MnBi₂Te₄. For samples with identical mass, the strength of magnetic signals in MnBi₄Te₇ will be 4 times weaker than those in MnBi₂Te₄. Therefore a good estimation of the background signal is crucial for the quantitative

analysis. Details of the background subtraction can be found in the supplementary information [27], including representative energy cuts of I(q, E) along (H, H, 0) and (-K, K, 0).

To account for magnon damping, cuts of I(q, E) were first fit to Eqn. (6) independently to obtain the damping parameter $\Gamma(E)$. $\Gamma(E)$ was then parameterized by the function $\Gamma(E) = c_1 \arctan(c_2E + c_3) + c_4$. In fits to the full 2D spectra, we keep the value of the single-ion anisotropy $SD_z = 0.077$ meV and $J_c = 0$, and let c_1, c_2, c_3, c_4 and intralayer interactions J_1, \ldots, J_9 vary freely. To account for the effects of summation in q, cuts of the simulations were made with the finite q-binning identical to the data and compared to the data cuts. A good fit is achieved when the reduced χ^2 (sum of all χ^2 divided by the number of fitting parameters) reaches minimum reduced $\chi^2 = 10.82$. The extracted intralayer interactions are compiled in Table. I, together with the values in MnBi₂Te₄ for comparison.

IV. DISCUSSION

In MnBi₂Te₄, previous reports find that the interlayer magnetic coupling J_c is relatively strong considering

TABLE I. Comparison of the strength of intralayer magnetic coupling SJ_{ij} (meV) in MnBi₄Te₇ and MnBi₂Te₄

	SJ_1	SJ_2	SJ_3	SJ_4	SJ_5	SJ_6	SJ_7	SJ_8	SJ_9
$MnBi_4Te_7$									-0.009(1)
$MnBi_2Te_4$	-0.233(2)	0.033(2)	-0.007(2)	0.003(1)	-0.016(2)	-0.013(2)	-0.008(1)	_	_

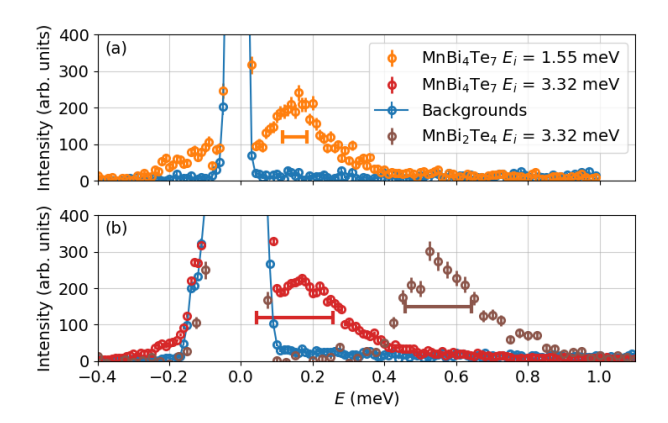


FIG. 3. Spin gap in MnBi₄Te₇ at the magnetic Γ point, compared to MnBi₂Te₄. Orange and red circles are INS intensities at $\boldsymbol{q}=(0,0,2.5)$, having $E_{\rm i}=1.55$ meV and 3.32 meV, respectively. Blue circles are at $\boldsymbol{q}=(0.3,0,2.5)$, demonstrating the incoherent background. Brown circles are INS intensities at $\boldsymbol{q}=(0,0,4.5)$ for MnBi₂Te₄. The horizontal bars show the instrumental resolution FWHM at peak center positions.

van der Waals nature of the magnetic coupling between $\mathrm{MnBi_2Te_4}$ blocks. The large spin gap ($\Delta\approx0.5~\mathrm{meV}$) is consistent with the presence of the relatively strong uniaxial anisotropy. When compared to critical fields for spin-flop and saturation transitions determined from magnetization measurements, we can conclude that the uniaxial anisotropy in $\mathrm{MnBi_2Te_4}$ has contributions from both single-ion anisotropy and anisotropy of the interlayer exchange coupling.

In MnBi₄Te₇, we find the interlayer coupling to be negligible within the sensitivity of our measurement, consistent with the larger separation between magnetic layers. However, AF interlayer exchange coupling must still exceed the dipolar interaction that favors a global FM order. We perform a lattice sum to estimate the net FM interlayer dipolar interaction, $J_{\rm c}^{\rm dip}=(g\mu_B)^2\frac{\mu_0}{4\pi}\sum_j\frac{r_{0j}^2-3(r_{0j}\cdot\hat{z})^2}{r_{0j}^5}$. By restricting the sum to include only interlayer bonds in the upper-half plane, we obtain $J_c^{\text{dip}} \approx -0.003 \text{ meV}$, which is smaller than the estimated upper limit of the total interlayer coupling that includes both exchange and dipolar terms $(J_{\rm c}=J_{\rm c}^{\rm ex}+J_{\rm c}^{\rm dip}\lesssim 0.01~{
m meV})$. This suggests that ${\rm MnBi_4Te_7}$ can still host AF order when interlayer AF exchange lies in an estimated range of $0.003 \lesssim J_c^{\text{ex}} \lesssim 0.013$. Ultimately, the interlayer AF exchange is exceeded by the dipolar interactions in MnBi₈Te₁₃ which crosses over to FM order [20].

We now discuss the magnetic anisotropy. The local

atomic configuration surrounding an Mn ion within a single septuple block is essentially the same for $\rm MnBi_2Te_4$ and $\rm MnBi_4Te_7$. Thus, we expect that the single-ion anisotropy in the two compounds should be similar and this is confirmed by our experimental data. In $\rm MnBi_2Te_4$, the overall anisotropy has contributions from interlayer exchange anisotropy, but this contribution will be reduced in $\rm MnBi_4Te_7$ due to the overall weaker exchange coupling.

Magnetization and transport data MnBi₄Te₇ are consistent with weaker interlayer AF coupling and dominant uniaxial magnetic anisotropy. Within the Stoner-Wohlfarth model, this weakening results in low-field spin-flip transitions with extremely low coercivity. This is borne out by magnetization and Hall measurements [9] where metamagnetism is heavily dominated by uniaxial anisotropy.

Finally, our results suggest that the intralayer interactions are transferable across the whole MBT family and play a decisive role in the magnetization dynamics of a single-layer magnet where n is large. The FM nearest-neighbor interaction J_1 is the dominant interaction, and a competing AFM J_2 somewhat destabilizes the FM Mn planes. Both systems also display a relatively long-range neighbor J_5 with comparable strength to J_2 . J_5 is in the same crystallographic a-axis direction as J_1 at distance of 3a and provides third order harmonics to J(q) that lead to the distinct linear dispersion relation along (H, 0, 0).

V. CONCLUSIONS

We have measured the spin wave dispersion of the antiferromagnetic topological insulator $\mathrm{MnBi_4Te_7}$. The interactions are strongly two-dimensional in character. However, the key magnetic energy scales within a single septuple block, the single-ion anisotropy and the intralayer exchanges, are transferable to all members of the MBT family.

ACKNOWLEDGEMENTS

This work is supported by the U.S. Department of Energy, Office of Basic Energy Sciences, Division of Materials Sciences and Engineering. Ames Laboratory is operated for the U.S. Department of Energy by Iowa State University under Contract No. DE-AC02-07CH11358. This research used resources at the Spallation Neutron Source, a DOE Office of Science User Facility operated by the Oak Ridge National Laboratory.

- [1] M. M. Otrokov, T. V. Menshchikova, M. G. Vergniory, I. P. Rusinov, A. Yu Vyazovskaya, Y. M. Koroteev, G. Bihlmayer, A. Ernst, P. M. Echenique, A. Arnau, et al., Highly-Ordered Wide Bandgap Materials for Quantized Anomalous Hall and Magnetoelectric Effects, 2D Mater. 4, 025082 (2017).
- [2] M. M. Otrokov, I. I. Klimovskikh, H. Bentmann, D. Estyunin, A. Zeugner, Z. S. Aliev, S. Gaß, A. U. B. Wolter, A. V. Koroleva, A. M. Shikin, et al., Prediction and Observation of an Antiferromagnetic Topological Insulator, Nature 576, 416 (2019).
- [3] J.-Q. Yan, Q. Zhang, T. Heitmann, Z. Huang, K. Y. Chen, J. G. Cheng, W. Wu, D. Vaknin, B. C. Sales, and R. J. McQueeney, Crystal growth and magnetic structure of MnBi₂Te₄, Phys. Rev. Mater. 3, 064202 (2019).
- [4] D. Zhang, M. Shi, T. Zhu, D. Xing, H. Zhang, and J. Wang, Topological Axion States in the Magnetic Insulator MnBi₂Te₄ with the Quantized Magnetoelectric Effect, Phys. Rev. Lett. 122, 206401 (2019).
- [5] Y. Deng, Y. Yu, M. Z. Shi, Z. Guo, Z. Xu, J. Wang, X. H. Chen, and Y. Zhang, Quantum anomalous Hall effect in intrinsic magnetic topological insulator MnBi₂Te₄, Science 367, 895 (2020).
- [6] C. Liu, Y. Wang, H. Li, Y. Wu, Y. Li, J. Li, K. He, Y. Xu, J. Zhang, and Y. Wang, Robust axion insulator and Chern insulator phases in a two-dimensional antiferromagnetic topological insulator, Nat. Mater. 19, 522 (2020).
- [7] A. Gao, Y.-F. Liu, C. Hu, J.-X. Qiu, C. Tzschaschel, B. Ghosh, S.-C. Ho, D. Bérubé, R. Chen, H. Sun et al. (2021). Layer Hall effect in a 2D topological axion antiferromagnet. Nature 595, 521 (2021).
- [8] S.K. Chong, Y. Cheng, H. Man, et al., Intrinsic exchange biased anomalous Hall effect in an uncompensated antiferromagnet MnBi₂Te₄, Nature Communications 15, 2881 (2024).
- [9] A. Tan, V. Labracherie, N. Kunchur, A. U. B. Wolter, J. Cornejo, J. Dufouleur, B. Büchner, A. Isaeva, and R. Giraud, Metamagnetism of Weakly Coupled Antiferromagnetic Topological Insulators, Phys. Rev. Lett. 124, 197201 (2020).
- [10] R. C. Vidal, A. Zeugner, J. I. Facio, R. Ray, M. H. Haghighi, A. U. B. Wolter, L. T. Corredor Bohorquez, F. Caglieris, S. Moser, T. Figgemeier et al., Topological Electronic Structure and Intrinsic Magnetization in MnBi₄Te₇:A Bi₂Te₃ Derivative with a Periodic Mn Sublattice, Phys. Rev. X 9, 041065 (2019).
- [11] J. Wu, F. Liu, M. Sasase, K. Ienaga, Y. Obata, R. Yukawa, K. Horiba, H. Kumigashira, S. Okuma, T. Inoshita et al., Natural van der Waals heterostructural single crystals with both magnetic and topological properties, Sci. Adv. 5, eaax9989 (2019).
- [12] J.-Q. Yan, Y. H. Liu, D. S. Parker, Y. Wu, A. A. Aczel, M. Matsuda, M. A. McGuire, and B. C. Sales, A-type antiferromagnetic order in MnBi₄Te₇ and MnBi₆Te₁₀ single crystals, Phys. Rev. Mater. 4, 054202 (2020).
- [13] L. Ding, C. Hu, F. Ye, E. Feng, N. Ni, and H. Cao, Crystal and magnetic structures of magnetic topological insulators MnBi₂Te₄ and MnBi₄Te₇, Phys. Rev. B 101,

- 020412 (2020).
- [14] I. I. Klimovskikh, M. M. Otrokov, D. Estyunin, S. V. Eremeev, S. O. Filnov, A. Koroleva, E. Shevchenko, V. Voroshnin, A. G. Rybkin, I. P. Rusinov et al., Tunable 3D/2D magnetism in the (MnBi₂Te₄)(Bi₂Te₃)_m topological insulators family, npj Quantum Mater. 5, 54 (2020).
- [15] M. Ceccardi, A. Zeugner, L. C. Folkers, C. Hess, B. Büchner, D. Marré, A. Isaeva, and F. Caglieris, Anomalous Nernst effect in the topological and magnetic material MnBi₄Te₇, Npj Quantum Mater. 8, 76 (2023).
- [16] J. Wu, F. Liu, C. Liu, Y. Wang, C. Li, Y. Lu, S. Matsuishi, and H. Hosono, Toward 2D Magnets in the (MnBi₂Te₄)(Bi₂Te₃)_n Bulk Crystal, Adv. Mater. 32, 2001815 (2020).
- [17] W. Ge, J. Kim, Y.-T. Chan, D. Vanderbilt, J. Yan, and W. Wu, Direct Visualization of Surface Spin-Flip Transition in MnBi₄Te₇, Phys. Rev. Lett. **129**, 107204 (2022).
- [18] G. Yu, C. Tang, Z. Tian, Z. Zhu, P. Liu, A. Pan, M. Chen, and X.-Q. Chen, Ferroelectrically Switchable Magnetic Multistates in MnBi₂Te₄(Bi₂Te₃)_n and MnSb₂Te₄(Bi₂Te₃)_n (n = 0,1) Thin Films, Phys. Rev. B 108, 014106 (2023).
- [19] J. Cui, B. Lei, M. Shi, Z. Xiang, T. Wu, and X. Chen, Layer-Dependent Magnetic Structure and Anomalous Hall Effect in the Magnetic Topological Insulator MnBi₄Te₇, Nano Lett. 23, 1652 (2023).
- [20] C. Hu, L. Ding, K. N. Gordon, B. Ghosh, H.-J. Tien, H. Li, A. G. Linn, S.-W. Lien, C.-Y. Huang, S. Mackey, J. Liu, P. V. S. Reddy, B. Singh, A. Agarwal, A. Bansil, M. Song, D. Li, S.-Y. Xu, H. Lin, H. Cao, T.-R. Chang, D. Dessau, et al., Realization of an Intrinsic Ferromagnetic Topological State in MnBi₈Te₁₃, Sci. Adv. 6, eaba4275 (2020).
- [21] J. Guo et al., Interlayer coupling modulated tunable magnetic states in superlattice MnBi₂Te₄(Bi₂Te₃)_n topological insulators, Phys. Rev. B 109, 165410 (2024).
- [22] Bing Li, D. M. Pajerowski, S. X. M. Riberolles, Liqin Ke, J.-Q. Yan, and R. J. McQueeney, Quasi-two-dimensional ferromagnetism and anisotropic interlayer couplings in the magnetic topological insulator MnBi₂Te₄, Phys. Rev. B 104, L220402 (2021).
- [23] Bing Li, J.-Q. Yan, D. M. Pajerowski, E. Gordon, A.-M. Nedić, Y. Sizyuk, L. Ke, P. P. Orth, D. Vaknin, and R. J. McQueeney, Competing Magnetic Interactions in the Antiferromagnetic Topological Insulator MnBi₂Te₄, Phys. Rev. Lett. **124**, 167204 (2020).
- [24] C. Lei, O. Heinonen, A. H. MacDonald, and R. J. Mc-Queeney, Metamagnetism of Few-Layer Topological Antiferromagnets, Phys. Rev. Mater. 5, 064201 (2021).
- [25] S. Yang, X. Xu, Y. Zhu, R. Niu, C. Xu, Y. Peng, X. Cheng, X. Jia, Y. Huang, X. Xu et al., Odd-Even Layer-Number Effect and Layer-Dependent Magnetic Phase Diagrams in MnBi₂Te₄, Phys. Rev. X 11, 011003 (2021).
- [26] C. Lei, T. V. Trevisan, O. Heinonen, R. J. McQueeney, and A. H. MacDonald, Quantum anomalous Hall effect in perfectly compensated collinear antiferromagnetic thin films, Phys. Rev. B 106, 195433 (2022).
- [27] See Supplementary Materials.